Effective interaction between helical biomolecules

E. Allahyarov[1,2] and H. Löwen[1]

[1]*Institut für Theoretische Physik II, Heinrich-Heine-Universität Düsseldorf, D-40225 Düsseldorf, Germany*
[2]*Institute for High Temperatures, Russian Academy of Sciences, 127412 Moscow, Russia*

The effective interaction between two parallel strands of helical biomolecules, such as deoxyribose nucleic acids (DNA), is calculated using computer simulations of the ''primitive'' model of electrolytes. In particular we study a simple model for B-DNA incorporating explicitly its charge pattern as a double-helix structure. The effective force and the effective torque exerted onto the molecules depend on the central distance and on the relative orientation. The contributions of nonlinear screening by monovalent counterions to these forces and torques are analyzed and calculated for different salt concentrations. As a result, we find that the sign of the force depends sensitively on the relative orientation. For intermolecular distances smaller than 6 Å it can be both attractive and repulsive. Furthermore, we report a nonmonotonic behavior of the effective force for increasing salt concentration. Both features cannot be described within linear screening theories. For large distances, on the other hand, the results agree with linear screening theories provided the charge of the biomolecules is suitably renormalized.

I. INTRODUCTION

Aqueous solutions of helical biomolecules like deoxyribose nucleic acids (DNA) are typically highly charged such that electrostatic interactions play an important role in many aspects of their structure and function [1–6]. Understanding the total effective interaction between two helical molecules is important since this governs the self-assembly of biomolecules, like bundle formation and DNA condensation or compaction which in turn is fundamental for gene delivery and gene therapy. In aqueous solution, such rodlike polyelectrolytes release counterions in the solution which ensure global charge neutrality of the system. Together with these counterions, there are, in general, added salt ions dissolved in the solution. The thermal ions screen the bare electrostatic interactions between the biomolecules, such that the effective interaction between them is expected to become weaker than the direct Coulomb repulsion. For very high concentrations of biomolecules or short distances even a mutual attraction due to counterion ''overscreening'' is conceivable [7–24].

In this paper, we study the effective interaction between two parallel helical biomolecules. In particular, we investigate how the electrostatic interactions are influenced by details of the charge pattern on the biological macromolecules. In fact, in many cases, as, e.g., for DNA molecules, the charge pattern on the molecules is not uniform but exhibits an intrinsic helix structure. If two parallel helical molecules are nearby, this helix structure will induce an interaction that depends on the relative orientation of the two helices. Our studies are based on computer simulation of the ''primitive'' model of electrolytes [25]. In particular we study a simple model for B-DNA. This model explicitly takes into account the double-helical charge pattern along the DNA strand, it also accounts for the molecular shape by modeling the major and minor grooves along the strand. The charged counterions and salt ions in the solutions are explicitly incorporated into our model. On the other hand, the water molecules only constitute a continuous background with a dielectric constant ϵ screening the Coulomb interactions. Hence the discrete nature of the solvent is neglected as well as more subtle effects as image charges induced by dielectric discontinuities at the DNA-water boundary [26–29], hydration effects due to the affection of the hydrophilic surface to the interfacial layers of water [30–35], and spatial dependent dielectric constants resulting from the decreasing water mobility in confining geometries and from saturation effects induced by water polarization near the highly charged molecular surfaces [36–41].

Our motivation to consider such a simple primitive model is threefold: First, though solvent effects seem to be relevant they should average out on a length scale which is larger than the range of the microscopic sizes. Hence the electrostatic effects are expected to dominate the total effective interactions. Second, it is justified to study a simple model completely and then adapt it by introducing more degrees of freedom in order to better match the experimental situation. Our philosophy is indeed to understand the principles of a simple model first and then turn step by step to more complicated models. Third, even within the primitive approach, there are many unsolved problems and unexpected effects such as mutual attraction of equally charged particles. Our computer simulation method has the advantage that ''exact'' results are obtained that reflect directly the nature of the model. Hence we get rid of any approximation inherent in a theoretical description. Consequently, the dependence of the effective interactions on a model parameter can systematically be studied and the trends can be compared to experiments. In this respect our model is superior to previous studies that describe the counterion screening by linear Debye-Hückel [39,42,4,43] or nonlinear Poisson-Boltzmann theory [26,4,44–51] and even to recent approaches that include approximatively counterion correlations [52,53]. We also emphasize that one main goal of the paper is to incorporate the molecular shape and charge pattern explicitly which is modeled in many studies simply as a homogeneously charged

cylinder [39,4,54,55]. In fact we find that the double-helix structure has an important influence on the effective interaction for surface-to-surface separations smaller than 6 Å. In detail, the interaction can be both repulsive and attractive depending on the relative orientation and the mutual distance between two parallel DNA strands. This effect which is typically ignored in the charged-cylinder model for DNA will significantly affect the self-assembly of parallel smectic layers of DNA fragments and may result in unusual crystalline structures at high concentrations.

Let us also mention that many theoretical studies involve only a single DNA molecule [56–59,3]. To extract the effective interaction, however, one has at least to include two molecules in the model which is the purpose of the present paper. In this study we only consider monovalent counterions. Multivalent counterions and a more detailed survey on the influence of model parameters on the effective interactions will be considered in a subsequent publication.

The remainder of paper is organized as follows. In Sec. II we present the details of the model used in this paper. Section III describes the target quantities of the applied model. Simulation details are presented in Sec. IV. Theories based on linear screening approaches such as the homogeneously charged cylinder model, the Yukawa segment model and the Kornyshev-Leikin theory [60] are shortly discussed in Sec. V. Results of the simulation and their comparison to linear screening theories are contained in Secs. VI–VIII for the point-charge model, the grooved model, and added salt, respectively. We conclude in Sec. IX.

II. THE MODEL

The charge pattern and the shape of a single B-DNA molecule is basically governed by the phosphate groups which exhibit a double-helix structure with right-hand helicity. We model this by an infinitely long neutral hard cylinder oriented in the z direction with additional charged hard spheres whose centers are located on the cylindrical surface. Each charged sphere describes a phosphate group and hence the spheres form a double-helix structure. In detail, the effective cylindrical diameter D is commonly chosen to be $D = 20$ Å [61,62,49]. The spheres are monovalent, i.e., their charge $q_p < 0$ corresponds to one elementary charge $e > 0$, $q_p = -e$, and they have an effective diameter d_p. We do not fix d_p but keep it as an additional (formal) parameter in the range between $d_p = 0.2$ Å (practically the pointlike charge limit) to $d_p = 6$ Å (to incorporate a groove geometry for the molecule). Furthermore, the helical pitch length is $P = 34$ Å; the number of charged spheres per pitch length (or per helical turn) is 20, with ten charges per strand. Consequently, successive charges on the same strand are displaced by an azimuthal angle of 36° corresponding to a charge spacing of 3.4 Å in z direction. In a plane perpendicular to the z direction, phosphate groups of the two different helices are separated by an azimuthal angle of $\phi_s = 144°$, see Fig. 1, fixing the minor and the major helical groove along the DNA molecule.

We place the discrete charges on the two different helices such that two of them fall in a common plane perpendicular to the z axis, see again Fig. 1. The total line charge density along the DNA molecule is then $\lambda = -0.59e/\text{Å}$.
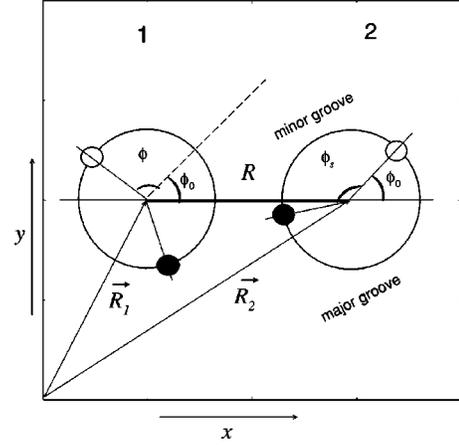
FIG. 1. A schematic picture explaining the positions of DNA molecules and the definition of the different azimuthal angles ϕ_0, ϕ, ϕ_s. For further information see text.

The second DNA molecule is considered to be parallel to the first one in our studies. The separation between the two cylinder origins is R; we also introduce the surface-to-surface separation $h = R - D$. The position of the two double helices can be described by a relative angle difference ϕ between the two azimuthal angles describing the position of the bottom helix with respect to a fixed axis in the xy plane. This is illustrated in Fig. 1. The relative orientation ϕ is the key quantity in describing the angle dependence of the forces induced by the helical structure. We remark that we only study a situation where the discrete phosphates from different DNA strands possess the same z coordinates for $\phi = 0$. Small shifts in the z coordinate are not expected to change the results significantly. A further parameter characterizing the discrete location of the phosphate charges along the strands is the azimuthal angle ϕ_0 of a phosphate charge with respect to the cylinder separation vector, see again Fig. 1. All results are periodic in ϕ_0 with a periodicity of 36°.

In addition to the DNA molecules we describe the counterions by charged hard spheres of diameter d_c and charge q_c. The counterions are held at room temperature $T = 298$ K. Their concentration is fixed by the charge of the DNA molecules due to the constraint of global charge neutrality. Also, additional salt ions with charges q_+ and q_-, modeled as charged hard spheres of diameters d_+ and d_-, are incorporated into our model. The salt concentration is denoted by C_s. The discrete nature of the solvent, however, is neglected completely.

The interactions between the mobile ions and phosphate charges are described within the framework of the primitive model as a combination of excluded volume and Coulomb interactions screened by the dielectric constant ϵ of the solvent. The corresponding pair interaction potential between the different charged hard spheres is

$$V_{ij}(r) = \begin{cases} \infty & \text{for } r \le (d_i + d_j)/2 \\ \dfrac{q_i q_j e^2}{\epsilon r} & \text{for } r > (d_i + d_j)/2, \end{cases} \quad (1)$$

where r is the interparticle separation and i,j are indices denoting the different particles species. Possible values for i

TABLE I. List of key variables.

D	DNA diameter
d_c	counterion diameter
d_p	phosphate diameter
d_+, d_-	salt ion diameters
P	helical pitch length
L	length of simulation box
ϵ	dielectric constant of DNA and water
T	temperature
N_p	number of phosphates in the simulation box
N_c	number of counterions in the simulation box
N_s	number of salt ion pairs in the simulation box
C_s	salt concentration
q_c	counterion valency
q_p	phosphate valency
q_+, q_-	salt ion valencies
λ	linear charge density of the DNA molecule
λ_B	Bjerrum length
Γ_{pc}	coupling parameter between phosphates and counterions
F	interaction force per pitch length
F_0	used unit for force, $F_0 = (\frac{e}{4D})^2$
M	torque acting onto the DNA molecules
R	interaxial separation between DNA molecules
h	surface-to-surface separation between DNA molecules
ϕ	relative orientational angle between two DNA molecules
ϕ_0	reference orientational angle for one DNA molecule
$F^{(HC)}$	interaction force per pitch length within the homogeneously charged cylinder model
λ_D	Debye screening length
$F^{(YS)}$	interaction force per pitch length within the Yukawa segment model
r_p^*	effective phosphate radius in the Yukawa segment model
q_p^*	effective phosphate charge in the Yukawa segment model
ζ	size correction factor in the Yukawa segment model
$F^{(KL)}$	interaction force per pitch length within Kornyshev-Leikin theory
θ	condensation parameter of counterions

and j are c (for counterions), $+,-$ (for positively and negatively charged salt ions), and p (for phosphate groups). In addition, there is an interaction potential V_i^0 between the DNA hard cylinder and the free ions $i=c,+,-$ which is of simple excluded volume form such that these ions cannot penetrate into the cylinder. Due to the length of this paper and the large number of quantities, we summarize most of our notation in Table I.

III. TARGET QUANTITIES

Our target quantities are equilibrium statistical averages for the local counterion and salt ion densities and the effective forces and torques exerted onto the biomolecules. For that purpose we consider a slightly more general situation with N parallel DNA molecules contained in a system of volume V. The cylinder centers are fixed at positions $\vec{R}_i (i = 1, \ldots, N)$ in the xy plane. We further assume that there are N_c counterions and N_+, N_- salt ions in the same system.

By this we obtain partial concentrations $n_c = N_c/V, n_+ = N_+/V, n_- = N_-/V$ of counterions and salt ions.

First we define the equilibrium number density profiles $\rho_j(\vec{r})(j=c,+,-)$ of the mobile ions in the presence of the fixed phosphate groups via

$$\rho_j(\vec{r}) = \left\langle \sum_{i=1}^{N_j} \delta(\vec{r} - \vec{r}_i^j) \right\rangle. \tag{2}$$

Here $\{\vec{r}_i^j\}$ denote the positions of the ith particle of species j. The canonical average $\langle \cdots \rangle$ over an $\{\vec{r}_i^j\}$-dependent quantity $\mathcal{A}$ is defined via the classical trace

$$\langle \mathcal{A} \rangle = \frac{1}{\mathcal{Z}} \left\{ \prod_{k=1}^{N_c} \int d^3 r_k^c \right\} \left\{ \prod_{m=1}^{N_+} \int d^3 r_m^+ \right\} \left\{ \prod_{n=1}^{N_-} \int d^3 r_n^- \right\}$$
$$\times \exp\left(-\beta \sum_{i=c,+,-} \left[V_i^0 + \sum_{j=c,p,+,-} U_{ij} \right] \right) \times \mathcal{A}. \tag{3}$$

Here $\beta = 1/k_B T$ is the inverse thermal energy (k_B denoting Boltzmann's constant) and

$$U_{ij} = (1 - \tfrac{1}{2}\delta_{ij}) \sum_{l=1}^{N_i} \sum_{k=1}^{N_j} V_{ij}(|\vec{r}_l^i - \vec{r}_k^j|) \tag{4}$$

is the total potential energy of the counterions and salt ions provided the phosphate groups are at positions $\{\vec{r}_n^p\}(n = 1, \ldots, N_p)$. Finally the prefactor $1/\mathcal{Z}$ in Eq. (3) ensures correct normalization, $\langle 1 \rangle = 1$. Note that the density profiles $\rho_j(\vec{r})$ also depend parametrically on the positions $\{\vec{r}_n^p\}$ of all the fixed phosphate groups ($n = 1, \ldots, N_p$).

Now we define the total effective force $\vec{F}_i$ per pitch length acting onto the ith DNA molecule ($i = 1, \ldots, N$). As known from earlier work [63,64,11,65] it contains three different parts

$$\vec{F}_i = \vec{F}_i^{(1)} + \vec{F}_i^{(2)} + \vec{F}_i^{(3)}. \tag{5}$$

The first term, $\vec{F}_i^{(1)}$, is the direct Coulomb force acting onto all phosphate groups belonging to one helical turn of the ith DNA molecule as exerted from the phosphate groups of all the other DNA molecules,

$$\vec{F}_i^{(1)} = -\sum_k{}' \left(\vec{\nabla}_{\vec{r}_k^p} \sum_{n=1;n\neq k}^{N_p} V_{pp}(|\vec{r}_k^p - \vec{r}_n^p|) \right), \tag{6}$$

where the sum Σ_k' only runs over ten phosphates belonging to one helical turn of the ith DNA molecule. This term is a trivial sum of direct interactions.

The second term $\vec{F}_i^{(2)}$ involves the electric part of the interaction between the phosphate groups and the counterions and salt ions. Its statistical definition is

$$\vec{F}_i^{(2)} = -\sum_k{}' \left(\left\langle \sum_{i=c,+,-} \sum_{l=1}^{N_i} \vec{\nabla}_{\vec{r}_k^p} V_{pi}(|\vec{r}_k^p - \vec{r}_l^i|) \right\rangle \right) \tag{7}$$

and describes screening of the bare Coulomb interaction (6) by the counterions and salt ions.

Finally, the third term $\vec{F}_i^{(3)}$ describes a contact (or depletion) force arising from the hard-sphere part in $V_{pi}(r)$ and $V_i^0 (i=c,+,-)$. It can be expressed as an integral over the molecular surface $\mathcal{S}_i$ associated with the excluded volume per one helical turn of the ith DNA molecule,

$$\vec{F}_i^{(3)} = -k_B T \int_{\mathcal{S}_i} d\vec{f} \left(\sum_{j=c,+,-} \rho_j(\vec{r}) \right), \qquad (8)$$

where $\vec{f}$ is a surface normal vector pointing outwards the DNA molecule. This depletion term is usually neglected in any linear electrostatic treatment but becomes actually important for strong Coulomb coupling Γ_{pc} as conveniently defined by [11,66,65]

$$\Gamma_{pc} = \left| \frac{q_p}{q_c} \right| \frac{2\lambda_B}{d_p + d_c}, \qquad (9)$$

with the Bjerrum length $\lambda_B = q_c^2 e^2 / \epsilon k_B T$. When Γ_{pc} is much larger than one, the Coulomb interaction dominates thermal interactions and counterion condensation may occur. For DNA molecules this is relevant as $d_p + d_c = 4-6$ Å and $\lambda_B = 7.14$ Å for a monovalent counterion in water at room temperature, resulting in a coupling parameter Γ_{pc} larger than one.

Our final target quantity is the total torque per pitch length acting onto the ith DNA molecule. Its component M_i along the z direction (with unit vector $\vec{e}_z$) can also be decomposed into three parts,

$$M_i = M_i^{(1)} + M_i^{(2)} + M_i^{(3)}, \qquad (10)$$

with

$$M_i^{(1)} = -\vec{e}_z \cdot \sum_k{}' \; \vec{r}_k^p \times \left(\vec{\nabla}_{\vec{r}_k^p} \sum_{n=1;n \neq k}^{N_p} V_{pp}(|\vec{r}_k^p - \vec{r}_n^p|) \right), \qquad (11)$$

$$M_i^{(2)} = -\vec{e}_z \cdot \sum_k{}' \; \vec{r}_k^p \times \left(\left\langle \sum_{i=c,+,-} \sum_{l=1}^{N_i} \vec{\nabla}_{\vec{r}_k^p} V_{pi}(|\vec{r}_k^p - \vec{r}_l^i|) \right\rangle \right), \qquad (12)$$

and

$$M_i^{(3)} = k_B T \vec{e}_z \cdot \int_{\mathcal{S}_i} d\vec{f} \times \vec{r} \left(\sum_{j=c,+,-} \rho_j(\vec{r}) \right). \qquad (13)$$

IV. COMPUTER SIMULATION

Our computer simulation was performed within a simple setup which is schematically shown in Fig. 2. We consider two parallel DNA molecules in a cubic box of length L with periodic boundary conditions in all three directions. Note that, the periodicity in x and y directions ensures infinite repetitions of DNA molecules outside simulation cell. Thus we are dealing with a finite concentration of DNA, rather than with an isolated pair of DNA molecules. L is chosen to be three times the pitch length P such that there are $N_p = 120$ phosphate charges in the box. The number of counte-

FIG. 2. Schematic view of the setup: Two cylindrically shaped DNA molecules with a distance R at positions $\vec{R}_1$ and $\vec{R}_2$ are placed parallel to the z axis inside a cube of length L. The large gray spheres are counterions of diameter d_c. The black spheres of diameter d_p, connected by the solid line, are phosphate charges on the cylindrical surface of diameter D. P is the pitch of DNA. Arrays $\vec{r}_p$ and $\vec{r}_c$ point to positions of phosphates and counterions. For the sake of clarity, the positions of added salt ions are not shown. There are periodic boundary conditions in all three directions.

rions $N_c = 120$ in the box is fixed by charged neutrality while the number of salt ions N_s is governed by its concentration C_s. The separation vector between the centers of the two molecules points along the x direction of the simulation box. The relative orientation is described according to our notation presented in Sec. II, see again Fig. 1.

We performed a standard molecular dynamic (MD) code with the velocity Verlet algorithm [67]. System parameters used in our simulations are listed in Table II. The time step Δt of the simulation was typically chosen to be $10^{-2} \sqrt{m d_m^3 / e^2}$, with m denoting the (fictitious) mass of the mobile ions, such that the reflection of counterions following the collision with the surface of DNA core cylinder and phosphates is calculated with high precision. For every run the state of the system was checked during the simulation time. This was done by monitoring the temperature, average velocity, the distribution function of velocities, and the total potential energy of the system. On average it took about 10^4

TABLE II. Parameters used for the different simulation runs. The Debye screening length λ_D, as defined by Eq. (15), and the Coulomb coupling Γ_{pc} are also given.

Run	d_c(Å)	d_p(Å)	N_s	$C_s(M)$	λ_D(Å)	Γ_{pc}
A	1	0.2			9.6	12
B	2	2			9.6	3.6
C	2	6			9.6	1.8
D	1	0.2	15	0.025	8.6	12
E	1	0.2	60	0.1	6.8	12
F	1	0.2	120	0.2	5.6	12
G	1	0.2	440	0.73	3.3	12
H	1	0.2	1940	3.23	1.7	12
I	2	2	120	0.2	5.6	3.6

MD steps to get into equilibrium. Then during 5×10^4–5×10^6 time steps, we gathered statistics to perform the canonical averages for calculated quantities.

The long-ranged nature of the Coulomb interaction was numerically treated via the efficient method proposed by Lekner [68]. A summary of this method is given in Appendix A. In order to save CPU time, the Lekner forces between pair particles were tabulated in a separate code before entering into the main MD cycle. The tabulation on a $510\times510\times510$ grid with spatial step $=0.1$ Å was done in the following manner. The first particle was fixed at the origin $(0,0,0)$ while the second charge was successively embedded on sites of the generated grid. Then the force components acting onto the first charge were calculated via the Lekner method. A force data file was created which was used as a common input for all subsequent MD runs. To decrease error coming from a finite grid length, the forces in the simulations were calculated using the four-step focusing technique [69].

V. LINEAR SCREENING THEORY

Linear screening theory can be used to get explicit analytical expressions for the effective interactions between helical biomolecules. These kind of theories, however, should only work for weak Coulomb coupling and thus represent a further approximation to the primitive model. Depending on the form of the fixed charge pattern characterizing the biomolecules, one obtains different approximations.

A. Homogeneously charged cylinder

The simplest approach is to crudely describe the biomolecule as a homogeneously charged cylinder. In this case, the effective interaction force per pitch length between two parallel rods reads [25]

$$\vec{F}\equiv\vec{F}^{(HC)}=\frac{2\lambda^2 P\lambda_D K_1(r/\lambda_D)}{\epsilon(D/2)^2 K_1^2[D/(2\lambda_D)]}\frac{\vec{r}}{r}. \qquad (14)$$

Here r is the axis-to-axis separation distance between cylinders, λ_D is the Debye-Hückel screening length fixed by

$$\lambda_D=\sqrt{\frac{\epsilon k_B T}{4\pi\gamma[n_c(q_c e)^2+n_+(q_+ e)^2+n_-(q_- e)^2]}}, \qquad (15)$$

where the factor $\gamma=1-V_{cyl}/V$ is a correction due to the fact that the mobile ions cannot penetrate into the cylindric cores which excludes a total volume V_{cyl}. Furthermore, $K_1(x)$ is a Bessel function of imaginary argument. Obviously, the torque is zero for this charge pattern.

B. Yukawa segment model

It is straightforward to generalize the traditional Debye-Hückel approach to a general charge pattern resulting in a Yukawa-segment (YS) model [27,70–74]. One phosphate charge interacts with another phosphate charge via an effective Yukawa potential [75]

$$U(r)=\frac{(q_p\zeta)^2 e^2}{\epsilon r}\exp(-r/\lambda_D). \qquad (16)$$

Here, ζ describes a size correction due to the excluded volume of the phosphate groups. This term is assumed to be of the traditional Derjaguin-Landau-Verwey-Overbeek (DLVO) form

$$\zeta=\exp(r_p^*\lambda_D)/(1+r_p^*\lambda_D), \qquad (17)$$

where $r_p^*=(d_p+d_c)/2$ is an effective phosphate radius for the phosphate counterion interaction. We remark that nonlinear screening effects and the excluded volume of the cylinder can also be incorporated by replacing the bare phosphate charge q_p with an effective phosphate charge q_p^* [27,71,76].

Using the same notation as in Sec. III, the total effective force per pitch length acting onto the ith biomolecule is

$$\vec{F}_i\equiv\vec{F}_i^{(YS)}=-\sum_k{}'\ \vec{\nabla}_{\vec{r}_k^p}\sum_{n=1;n\neq k}^{N_p}U(|\vec{r}_k^p-\vec{r}_n^p|) \qquad (18)$$

within in the Yukawa segment model where the sum Σ' has the same meaning as in Eq. (6). Note that the contact term (8) is typically neglected in linear screening theory. Furthermore, the effective torque per pitch length is

$$M_i\equiv M_i^{(YS)}=-\vec{e}_z\cdot\sum_k{}'\ \vec{r}_k^p\times\left(\vec{\nabla}_{\vec{r}_k^p}\sum_{n=1;n\neq k}^{N_p}U(|\vec{r}_k^p-\vec{r}_n^p|)\right). \qquad (19)$$

There are also analytical expressions for the equilibrium density profiles of the mobile ions involving a linear superposition of Yukawa orbitals around the phosphate charges [77] which, however, we will not discuss further in the sequel.

C. Kornyshev-Leikin theory

The linear Debye-Hückel screening theory was recently developed further and modified to account for dielectric discontinuities and counterion adsorption in the grooves of the DNA molecule by Kornyshev and Leikin (KL) [60,78–81]. An analytical expression for the effective pair potential $V_{KL}(R,\phi)$ per pitch length between two parallel rods of separation R with relative orientation ϕ was given for separations larger than $R>D+\lambda_D$. Here we only discuss the leading contribution in the special case of no dielectric discontinuity which reads

$$V_{KL}(R,\phi)=\frac{8P\lambda^2}{\epsilon D^2}\sum_{n=-\infty}^{\infty}(-1)^n\frac{P_n^2\cos(n\phi)K_0(k_n R)}{k_n^2(1-\beta_n)^2[K_n'(k_n D/2)]^2} \qquad (20)$$

and corresponds to the interaction of helices whose strands form continuously charged helical lines. In Eq. (20),

$$\beta_n=\frac{ng}{k_n}\frac{K_n(k_n D/2)I_n'(ngD/2)}{K_n'(k_n D/2)I_n(ngD/2)}, \qquad (21)$$

$$k_n = \sqrt{1/\lambda_D^2 + (ng)^2}, \quad g = \frac{2\pi}{P}, \qquad (22)$$

K_n and I_n are modified Bessel functions of nth order, and $K_n'(x) = dK_n(x)/dx$, $I_n'(x) = dI_n(x)/dx$.

We emphasize that the KL theory does not assume *a priori* the double helical phosphate charge pattern as defined in Sec. II. There are rather more possible charge patterns considered, including a condensation of counterions in the minor and major groove along the phosphate strands, and on the cylinder as a whole. This involves four phenomenological parameters as a further input for the KL theory which makes a direct comparison to the simulation data difficult. In fact, for the charge pattern given in Sec. II, the KL theory reduces to the Yukawa-segment model.

In detail, the charge pattern is characterized by the form factor P_n,

$$P_n = (1 - f_1 - f_2 - f_3)\theta\delta_{n,0}$$
$$+ f_1\theta + f_2(-1)^n\theta - (1 - f_3\theta)\cos(n\phi_s).$$

Here $\delta_{n,m}$ is the Kronecker's delta function; θ is the first phenomenological input parameter which describes the fraction of counterions that are condensed on the whole cylinder. The three numbers f_i denote the fractions of counterions in the middle of the minor groove (f_1), in the middle of the major groove (f_2), and on the phosphate strands (f_3) with respect to all condensed counterions. We note that the sum in Eq. (20) rapidly converges, such that it can safely be truncated for $|n| > 2$. It is straightforward to obtain the effective force and torque per pitch length between two molecules from Eq. (20) by taking gradients with respect to R and ϕ.

VI. RESULTS FOR POINTLIKE CHARGES AND NO ADDED SALT

In what follows, we consider the set-up of two parallel biomolecules with periodic boundary conditions shown in Fig. 2. We projected $\vec{F}_1$ onto the vector $\vec{R}$, defining $F = \vec{F}_1 \cdot (\vec{R}_1 - \vec{R}_2)/|\vec{R}_1 - \vec{R}_2|$. Hence a negative sign of F implies attraction, and a positive sign repulsion. The torque is given for the first DNA molecule, hence $M \equiv M_1$. We start with the case of no added salt. First, we assume the counterion and phosphate diameters to be small, in order to formally investigate the system with a high coupling parameter $\Gamma_{pc} > 10$.

A. Distribution of the counterions around the DNA molecules

We calculated the equilibrium density field (2) of the counterions in the vicinity of the DNA molecules by computer simulation. In detail, we considered three different paths to show the counterion density profile around the first DNA molecule: along a phosphate strand and along the minor and major groove. In order to reduce the statistical error we course grained this density field further in a finite volume which is illustrated in Fig. 3.

This volume is winding around the molecules with a height ξ and width δ. We choose $\xi = 3.4$ Å and $\delta = 2$ Å
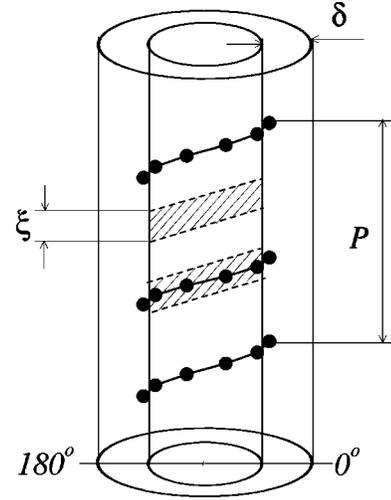
FIG. 3. A schematic picture to explain the procedure of counterion density calculations along one pitch length of a DNA molecule. The filled circles connected with the solid line are phosphate groups. The shaded areas correspond to a path along the major groove and along one phosphate strand. The considered volume has a height ξ and width δ. The neighboring DNA molecule is assumed to be on the right-hand side.

$+ d_c/2$. In Fig. 4 we plot this coarse-grained density field $\rho_c(\varphi)$ versus the azimuthal angle angle φ from 0° to 360° where φ is 0°, respectively, 360° in the inner region between the DNA molecules.
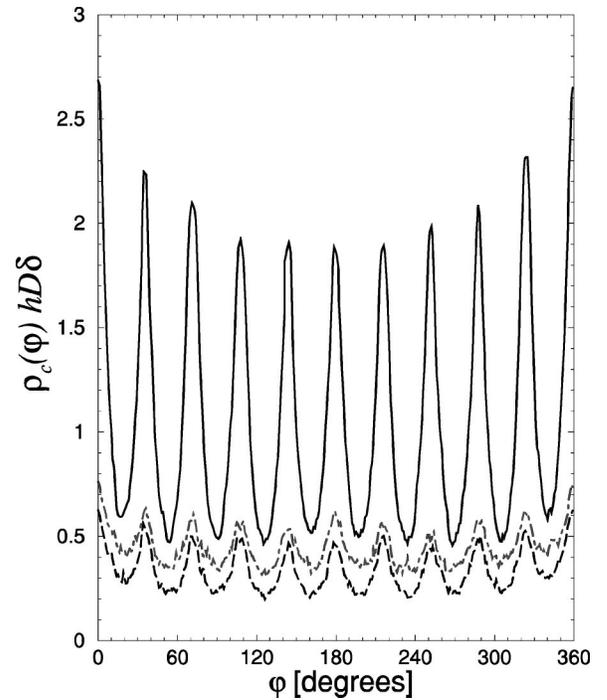
FIG. 4. Equilibrium counterion density profile $\rho_c(\varphi)$ in units of $1/hD\delta$ versus the azimuthal angle φ for the parameters of run A, $\phi = 0°$ and a rod separation of $R = 30$ Å. Solid line: counterion density profile along a phosphate strand (due to symmetry, the counterion density profiles on the two phosphate strands are the same). Dashed line: counterion density profile along the major groove. Dot-dashed line: counterion density profile along the minor groove.
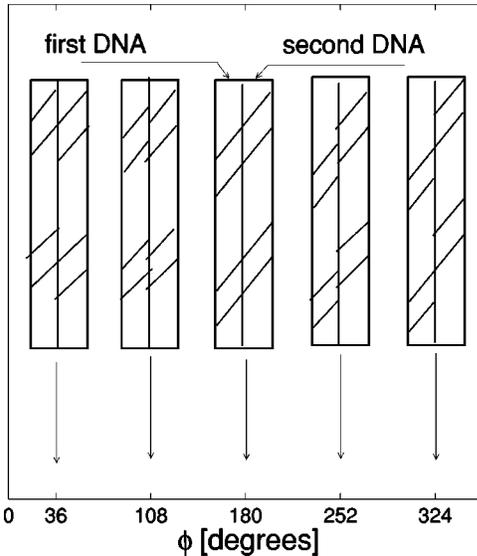
FIG. 5. Schematic picture of a DNA-DNA configuration for close separation distances. The abscissa corresponds to the rotation angle of the first DNA molecule. The second DNA molecule is fixed.

Obviously, the counterion density profile has maxima in the neighborhood of the fixed phosphate charges. Furthermore, the concentration of counterions is higher in the minor than in the major grooves with the φ dependence reflecting again the position of the phosphate charges. Also in the inner region between the two DNA molecules, there are on average more counterions than in the outside region.

B. Nearly touching configurations

Let us now consider very small surface-to-surface separations between the DNA molecules. In this case one expects that the dependence of the forces and torques on the relative orientation ϕ is most pronounced. For such nearly touching configurations, however, the discreteness of the phosphate charges, as embodied in the parameter ϕ_0, strongly influences the results as well. The qualitative behavior of the ϕ dependence can be understood from Fig. 5. Here two touching DNA molecules are shown for different relative orientations ϕ where the phosphate strands are schematically drawn as continuous lines. For certain angles ϕ that we call touching angles, two neighboring phosphate charges hit each other. Possible touching angles are $\phi=36°,180°,324°$. If ϕ_0 is chosen to be zero, then two point charges are opposing each other directly. Hence a strong dependence on ϕ and on ϕ_0 is expected near touching angles.

Results from computer simulation and YS theory are presented in Fig. 6. The parameters are from run A (see Table II) but with $d_c=0.8$ Å. The surface-to-surface separation is $h=2$ Å.

For touching angles the interaction force becomes strongly repulsive. The strongest repulsion is achieved for $\phi=180°$ since two phosphate strands are meeting simultaneously. For relative orientations different from a touching angle, the force becomes smaller and can be both, attractive and repulsive. YS theory always predicts a repulsive force. Again there are strong peaks for touching angles in qualita-
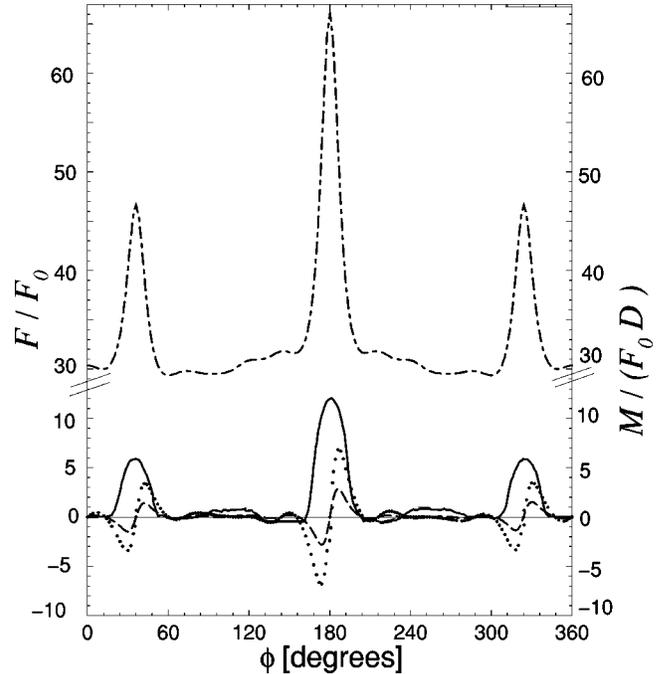
FIG. 6. Interaction force F (left y axis) and torque M (right y axis) for fixed surface distance $h=2$ Å versus relative orientation ϕ in degrees. The unit of the force is $F_0=(e/4D)^2$. The solid (dashed) line is the simulation result for $F(M)$ while the dot-dashed (dotted) line is data from the YS theory for $F(M)$. ϕ_0 is chosen to be zero. The counterion diameter is $d_c=0.8$ Å.

tive agreement with the simulation. The actual numbers predicted by the YS theory, however, are much too large and off by a factor of 6–7 around touching angles.

The torque shows an even richer structure as a function of ϕ. Near a touching angle it exhibits three zeroes corresponding to an unstable minimum exactly at the touching angle and two stable minima near the touching angles. The YS theory shows two times larger values for the torque as compared to the simulation data.

A qualitatively different force-angle behavior is observed for a larger counterion diameter. Results for $d_c=1$ Å are shown in Fig. 7.

Here at touching angles, the interaction force is attractive. The physical reason for that are the contact forces as given by Eq. (8). Caused by the larger counterion diameter, counterions are stronger depleted in the zone between the DNA molecules. The torque has qualitatively the same behavior as before.

We emphasize that the results do also depend strongly on ϕ_0. For $\phi_0=18°$, for instance, the force F practically vanishes for any relative orientation ϕ as compared to the same data for $\phi_0=0°$.

C. Distance-resolved forces

We now discuss in more detail the distance-resolved effective forces. For the parameters of run A, simulation results for F are presented in Fig. 8.

For $\phi_0=0$, the force depends on the relative orientation ϕ up to a surface-to-surface separation $h\approx6$ Å in accordance with Fig. 7. On the other hand, for $\phi_0=18°$, there is no ϕ
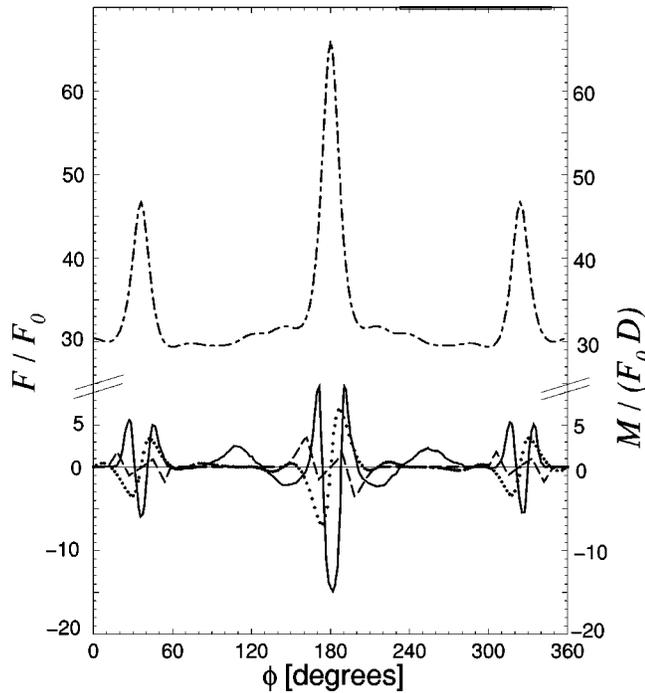
FIG. 7. Same as Fig. 6 but now for $d_c = 1$ Å.

dependence at all for any separation. This supports the conclusion of previous works [57,55] that the effect of discreteness of the DNA phosphate charges on the counterion concentration profile is small in general and dwindles a few Angstroms from the DNA surface. In fact, for $h > 6$ Å, there is neither a ϕ nor a ϕ_0 dependence of the force, and the total force is repulsive.
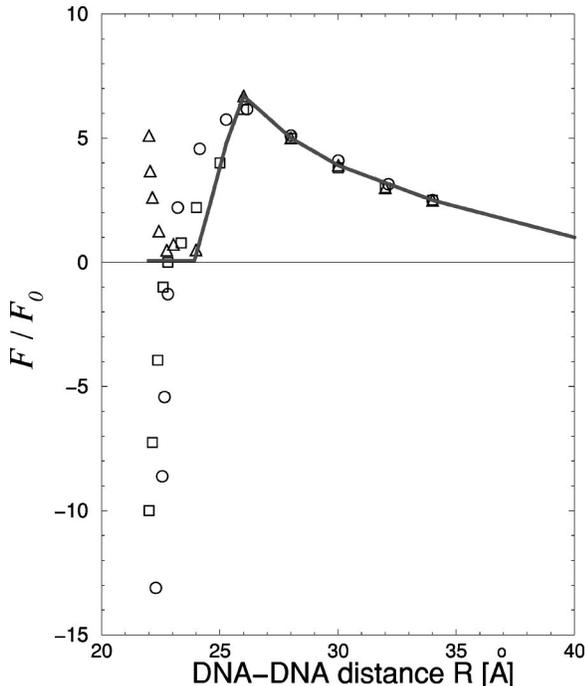
FIG. 8. Effective interaction force F acting onto a DNA pair versus the center-to-center distance R. The solid line is for $\phi_0 = 18°$. In this case there is no significant ϕ dependence. The meaning of the symbols that correspond to $\phi_0 = 0$ is circles, $\phi = 180°$; squares, $\phi = 36°$; triangles, $\phi = 45°$.
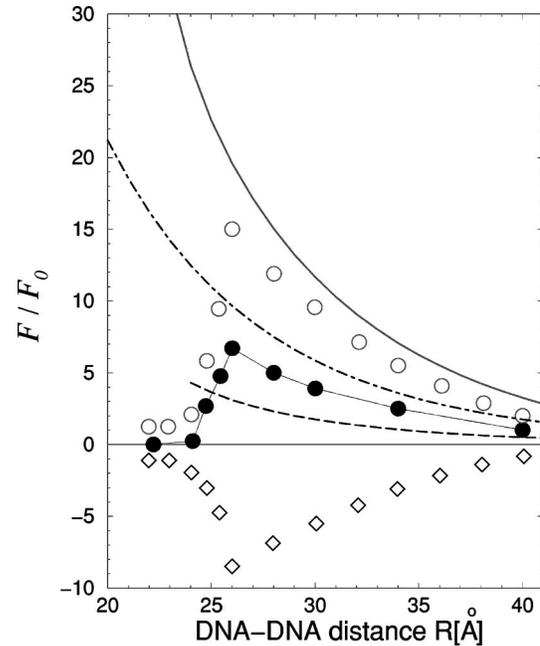
FIG. 9. Theoretical and simulation results for interaction force F versus separation distance R. The unit of the force is $F_0 = (e/4D)^2$. The parameters are from run A and $\phi_0 = 18°$. Symbols: $\bullet$, simulation data for all DNA rotation angles; $\bigcirc$, the entropic part $\vec{F}^{(3)}$; $\diamondsuit$, the pure electrostatic part $(\vec{F}^{(1)} + \vec{F}^{(2)})$. Solid line: YS theory. Dot-dashed line: homogeneously charged cylinder model. Dashed line: the predictions of KL theory with $f_1 = 0.1, f_2 = 0.1, f_3 = 0.7, \theta = 0.71$.

Furthermore, we compare our simulation results with the prediction of linear screening theories in Fig. 9. First of all, our simulation data for the total force (solid circles) are decomposed into the electrostatic part $F^{(1)} + F^{(2)}$ (diamonds) and the contact (or depletion) part $F^{(3)}$ (open circles). While the latter is strongly repulsive, the electrostatic part is attractive such that the net force is repulsive. Linear screening theories aim to describe the pure electrostatic force only.

As is seen from the plot in Fig. 9, the contact force has a nonmonotonic behavior. The physical reason for this is as follows: For decreasing separations R, more and more counterions are attracted towards the inner region between the molecules leading to a contact force that is increasing with decreasing distance. Then a threshold at ≈ 26 Å is reached where the counterions in the inner region start to feel their mutual repulsion. This, in turn, depletes the zone between the molecules from counterions resulting in a decreasing contact force upon further decreasing the distance R.

Results for linear screening theories on different levels are also collected in Fig. 9. If one compares with the *total* force, the prediction obtained by a homogeneously charged cylinder is repulsive and off by a factor of roughly 1.5. A simulation with a homogeneously charged rod yields perfect agreement with linear screening theory since the Coulomb coupling is strongly reduced as the rod charges are now in the inner part of the cylinder. The Yukawa-segment theory is repulsive and off by a factor of 3. It is understandable that the YS model leads to a stronger repulsion than the charged cylinder model as the separation of the phosphate charges in the inner region between the DNA molecules is shorter than the rod center separation.
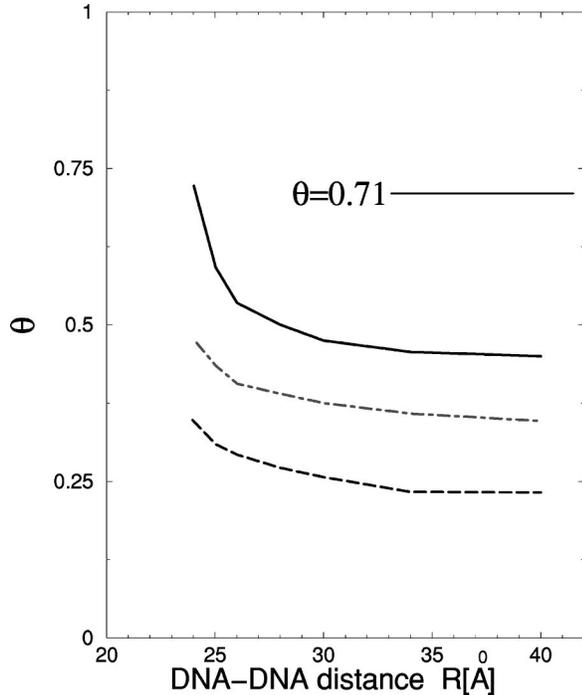
FIG. 10. The condensation parameter θ versus separation distance R. From top to bottom: solid line, run A ($d_c=1$ Å, $d_p=0.2$ Å); dot-dashed line, run B ($d_c=2$ Å, $d_p=2$ Å); dashed line, run C ($d_c=2$ Å, $d_p=6$ Å). The horizontal line at $\theta=0.71$ indicates the saturation value at large distances for a larger $\delta=l_B=7.1$ Å. This saturation value is the same for runs A, B, and C.

The Kornyshev-Leikin theory requires four counterion condensation fractions θ, f_1, f_2, f_3 as an input. We have tried to determine these parameters from our simulation in order to get a direct comparison without any fitting procedure. In order to do so, we introduce a shell around the cylinder of width δ and determine θ as the fraction of counterions which are contained within this shell. The number of ions in the shell is just meant as a measure for the presence of ions in the neighborhood of the surface. The actual value for δ is somewhat arbitrary; we first took a microscopic shell of width $\delta=2$ Å$+d_c/2$ (thus $\delta=2.5$ Å for run A and $\delta=3$ Å for runs B and C) as defined in Sec. VI A. Data for θ versus the rod separation are included in Fig. 10 for three different combinations of counterion and phosphate diameters. It becomes evident that the fraction θ of condensed counterions decreases with the rod distance but saturates at large separations. θ also depends on the size of the counterions and phosphate charges. Additionally for large surface-to-surface separations, $h>2\lambda_B$, we counted counterions within both $\delta=2$ Å$+d_c/2$ and $\delta=\lambda_B=7.1$ Å shells. For the latter case, the condensation fraction θ does not depend from separation distance and is constant for different combination of phosphate and counterion sizes; see the horizontal line $\theta=0.71$ in Fig. 10. This value of θ is comparable with Manning's condensation parameter [82,83] $\theta_0=1-|q_c|/\lambda\lambda_B=0.76$, which is the fraction of monovalent counterions approximately 7 Å beyond the surface of cylindrical DNA (and typically 17 Å from helix axis) [1,38]. Our data are also in semiquantitative accordance with other computer simulations [38] and nuclear magnetic resonance (NMR) experiments which show that the condensed counterion frac-

tions are in the range of 0.65 to 0.85 [84] or 0.53 to 0.57 [85,45].

According to our results for the counterion density distribution (see Fig. 4) we fix the minor and major groove fractions to $f_1=0.1, f_2=0.1$, and the strand fraction to $f_3=0.7$. Thus, $(1-f_1-f_2-f_3)=0.1$ is the fraction of the condensed counterions which is distributed neither on the phosphates strands nor on the minor and major grooves. The force in KL theory depends sensitively on θ but is rather insensitive with respect to f_1, f_2, f_3, and ϕ. If the Bjerrum length is taken as a width for the condensed counterions, $\theta=0.71$, then the KL theory underestimates the total force. If, on the other hand, a reduced value of $\theta=0.545$ is heuristically assumed, then the KL theory reproduces the total force quite well.

A serious problem of the comparison with linear screening theories is that the contact term is not incorporated in any theory apart from recent modifications [86,64]. In fact, one should better compare the pure electrostatic part which is attractive in the simulation. Consequently, none of the linear screening theories is capable to describe the force well. This is due to the neglection of correlations and fluctuations in linear screening theories. From a more pragmatic point of view, however, one may state that a suitable charge renormalization leads to quantitative agreement with the *total* force. In fact, all three theories yield perfect agreement if the phosphate charges, respectively, the condensation parameter θ, are taken as a fit parameter. For instance, the YS model yields perfect agreement with the simulation for distances larger than 26 Å if in Eq. (16) a renormalized phosphate charge $q_p^*=-0.6e$ is taken replacing the bare charge q_p. Thus, only two model parameters (λ_D and q_p) are sufficient to describe the interaction satisfactorily which is *a priori* not evident. But this is still unsatisfactory from a more principal point a view.

VII. RESULTS FOR THE GROOVED MODEL

The groove structure of DNA is expected to be of increasing significance as one approaches its surface [87]. We incorporate this in our model by increasing the phosphate diameter towards $d_p=2$ Å (run B) and $d_p=6$ Å (run C). Results for the condensation parameter θ are shown in Fig. 10. θ is decreasing with increasing d_p since the coupling parameter Γ_{pc} is decreasing which weakens counterion binding to the phosphate groups. Also the qualitative shape of the counterion density profiles depends sensitively on the groove nature as can be deduced from Fig. 11 as compared to Fig. 4. The counterion density along the phosphate strands now exhibits minima at the phosphate charge positions while it was maximal there in Fig. 4. Furthermore, the counterion density in the minor grooves is now higher than along the strands due to the geometrical constraints for the counterion positions which is similar to results of Ref. [55]. In fact, recent x-ray diffraction [88–90] and NMR spectroscopy [91,92] experiments, as well as molecular mechanics [93,94] and Monte Carlo simulations [5] suggest that monovalent cations selectively partition into the minor groove. This effect is present also in our simple model and can thus already be understood from electrostatics and thermostatics.

An increasing phosphate and counterion size increases the
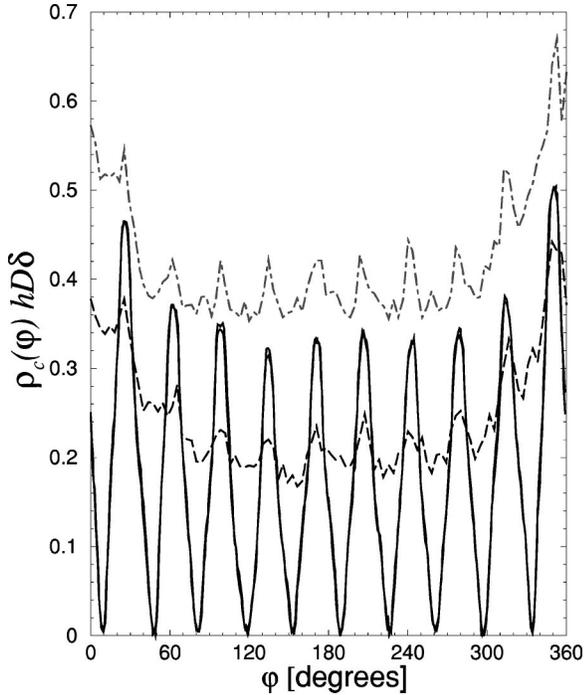
FIG. 11. Same as Fig. 4 but now for run C and $\phi=45°$, $\delta=3$ Å.

effective forces which is shown in Fig. 12. Here, as ϕ_0 was chosen to be 18°, there is no notable dependence on the relative orientation ϕ. A similar behavior was observed in a hexagonally ordered DNA system via Monte Carlo calculations [24]. This is understandable as counterion screening is becoming less effective. We have tried to fit the simulation data using a renormalized charge in the YS theory. A good fit was obtained for large separations while there are increasing deviations at shorter distances. This is different from our results for small ion sizes also shown in Fig. 12 where the fit was valid over the whole range of separations. The adjustable parameter q_p^* is shown versus the effective phosphate radius r_p^* of the YS model in the inset of Fig. 12. It is increasing with increasing r_p^* in qualitative agreement with charge renormalization models [95].

We also note that the physical nature of the electrostatic part of the interaction force undergoes a transformation upon decreasing the coupling parameter Γ_{pc}. For strong coupling, $\Gamma_{pc}=12$ (run A), the electrostatic part $F^{(1)}+F^{(2)}$ is attractive (see Fig. 9). For moderate coupling, $\Gamma_{pc}=3.6$ (run B), it is nearly zero for all distances. Finally, for weak coupling, $\Gamma_{pc}=1.8$ (run C) the electrostatic part is elsewhere repulsive. The entropic part $F^{(3)}$ for these three runs is always repulsive and does not undergo a significant change.

VIII. RESULTS FOR ADDED SALT

Interactions involving nucleic acids are strongly dependent on salt concentration. Indeed, the strength of binding constants can change by orders of magnitude with only small changes in ionic strength [96,97]. Our simulations show a similar strong salt impact on the interaction force.

When salt ions are added, there is a competition between two effects. The first one is the increasing of the direct re-

pulsion between molecules as a consequence of *delocalizing* the condensed counterions. The second stems from the osmotic pressure of added salt that pushes the salt ions to occupy the inner molecular region and to *screen* the DNA-DNA repulsion. As we shall show below, these two effects result in a novel non monotonic behavior of the force as a function of salt concentration.

Simulation results for F versus distance for increasing salt concentration are presented in Fig. 13. In our simulations, counterions and equally charged salt ions are indistinguishable. We take $d_+=d_-=d_c,|q_+|=|q_-|=e$. It can be concluded from Fig. 13 that even a small amount of salt ions (line 1, run D, $C_s=0.025M$) significantly enhances the DNA-DNA repulsion (compare with the dashed line corresponding to run A, $C_s=0M$). Upon increasing the salt concentration, at large separations, $h>10$ Å, the screening is increased in accordance with the linear theory. However, at intermediate and nearly touching separations, a nonmonotonic behavior as a function of salt concentration is observed as illustrated in the inset of Fig. 13. In the inset, the maximum of F occurs for $C_s=0.2M$. The physical reason for that is that added salt ions first delocalize bound counterions which leads to a stronger repulsion. Upon further increasing the salt concentration, the electrostatic screening is enhanced again and the force gets less repulsive. In order to support this picture we show typical microion configurations and investigate also the fraction θ of condensed counterions as a function of salt concentration.

Simulation snapshots are given in Fig. 14, where the positions of the mobile ions are projected onto the xy plane. A
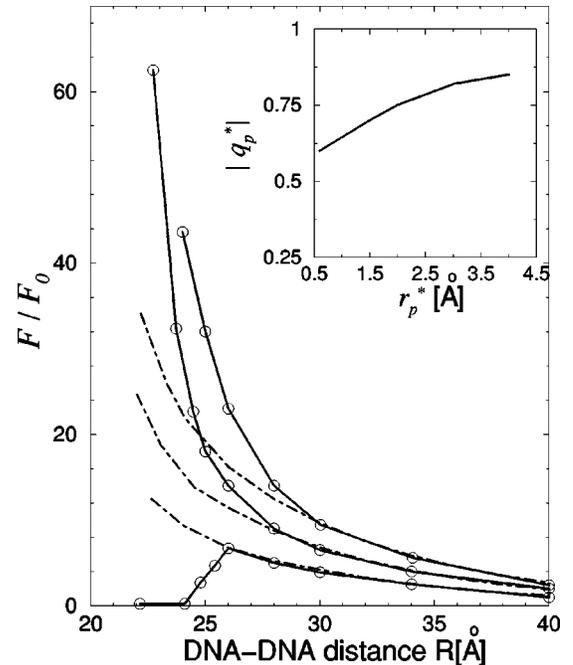
FIG. 12. Interaction force F versus separation distance R. The open circles are simulation data for all relative orientations ϕ with $\phi_0=18°$. From bottom to top: $d_c=1$ Å, $d_p=0.2$ Å (run A); $d_c=2$ Å, $d_p=2$ Å (run B); $d_c=2$ Å, $d_p=6$ Å (run C). The dashed lines are fits by the YS model. From bottom to top: fit for the parameters of run A with $q_p^*=-0.6e$; fit for the parameters of run B with $q_p^*=-0.75e$; fit for the parameters of run C with $q_p^*=-0.85e$. The inset is the variation of the renormalized phosphate charge q_p^* versus effective phosphate radius r_p^*.
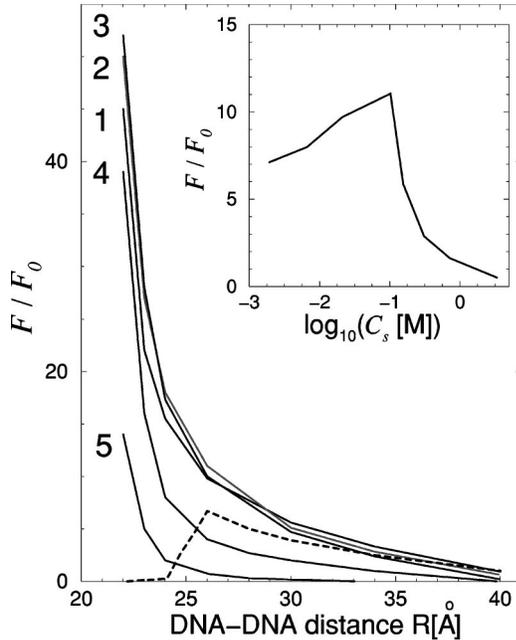
FIG. 13. Interaction force F acting onto a DNA pair versus distance for $\phi=0°$ and $\phi_0=18°$. The unit of the force is $F_0 = (e/4D)^2$. The solid lines are for increasing salt concentration: 1, run D; 2, run E; 3, run F; 4, run G; 5, run H. Dashed line: reference data without salt from run A. The inset shows the force versus salt concentration at fixed separation $R=26$ Å.

comparison of the salt-free case [Fig. 14(a)] with that of moderate salt concentration [$C_s=0.2M$, Fig. 14(b)] reveals that the total number of condensed counterions decreases with increasing C_s. Furthermore, for $C_s=0.2M$ [Fig. 14(b)], there are no coions in the inner DNA-DNA region. Thus coions do not effectively participate in screening. Consequently, the DNA-DNA interaction, due to delocalization of counterions, will be enhanced. Contrary to that, for $C_s =0.73M$ [Fig. 14(c)] the salt coions and counterions enter into the inner DNA-DNA region and effectively screen the interaction force.

Further information is gained from the fraction θ of condensed counterions which is plotted as a function of R for different salt concentrations C_s in Fig. 15. We define θ as the ratio of the net charge in terms of an elementary charge within the shell of δ with respect to the total number of counterions stemming from the molecule. As C_s increases, the saturation of θ occurs at smaller distances. In the inset of Fig. 15 a nonmonotonic behavior of θ as a function of the added salt concentration is visible which again is a clear signature of the scenario discussed above.

To understand the nonmonotonicity better, we performed additional simulations for a single DNA molecule in monovalent salt, runs D–H. As a result, the nonmonotonicity is present also for a single DNA if the shell width δ is not larger than 10 Å. The smaller δ, the most pronounced the nonmonotonicity. We have also performed simulation for a homogeneously charged rod. In this case, as the Coulomb coupling is much smaller, the nonmonotonicity of $\theta(C_s)$ vanishes. One can conclude that the nonmonotonicity of $\theta(C_s)$ is a consequence of the high Coulomb coupling, since
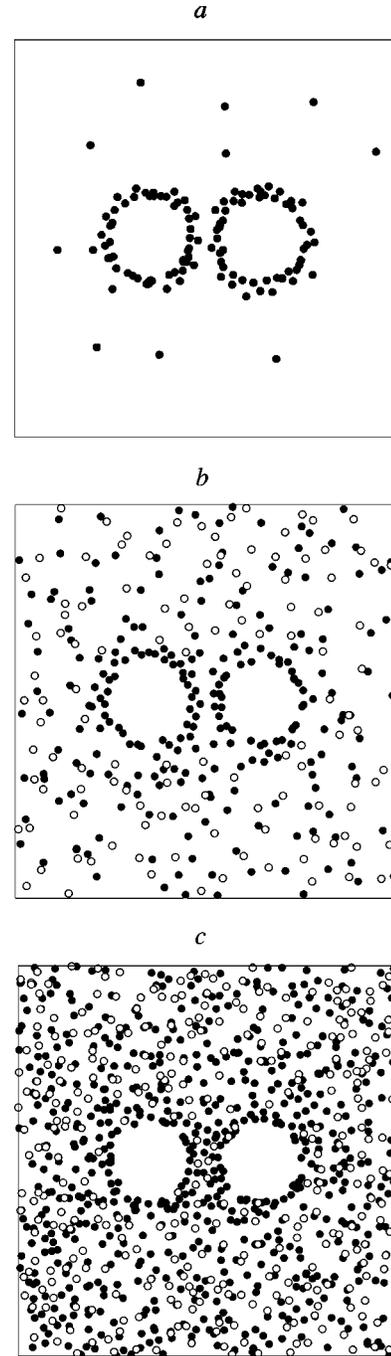
FIG. 14. Two-dimensional microion snapshots projected to a plane perpendicular to the helices for $\phi=0°$, $\phi_o=18°$, $R=30$ Å. The filled circles are the positions of the counterions and positive salt ions; the open circles are the positions for the negative salt ions (coions). a, run A; b, run F; c, run G.

$\Gamma_{pc}=12$ for a DNA molecule and $\Gamma_{pc}=0.7$ for a charged rod.

The increase of θ above a certain threshold of salt concentration is mainly due to a counterion accumulation outside the grooves. A similar trend was predicted by Poisson-Boltzmann [98] and Monte Carlo [61,47] calculations in different models.

More details of the forces and the comparison to linear screening theories are shown in Figs. 16, 17, and 18. For run F, the different parts of the total force are presented in Fig.
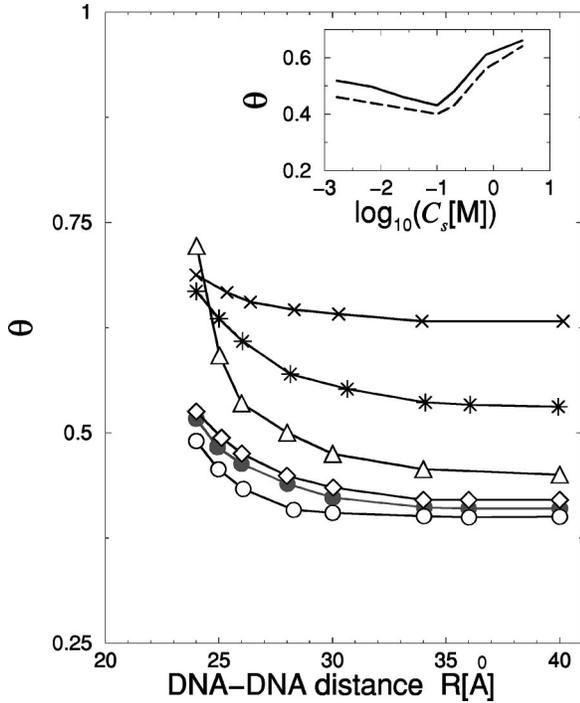
FIG. 15. Same as Fig. 10, but now with added salt. Symbols: △, run A; ●, run D; ○, run E; ◇, run F; *, run G; ×, run H. The inset shows θ for fixed distance as a function of salt concentration: solid line, for $R=26$ Å; dashed line, for $R=30$ Å.

16. As compared to the salt-free case (Fig. 9) the pure electrostatic part is again attractive but much smaller, while the depletion part is repulsive and dominates the total force. All three linear models, homogeneously charged cylinder model, YS, and KL theory, underestimate the force. Note that the
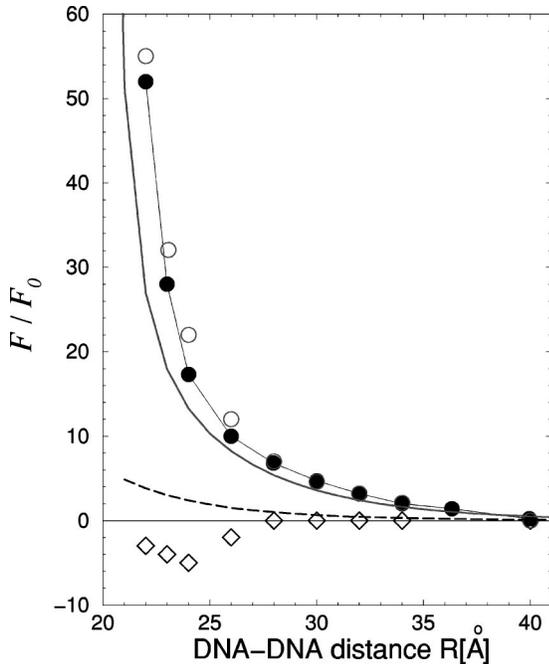
FIG. 16. Same as Fig. 9 but now for run F and $\phi=0°$, $\phi_0 =18°$. The KL theory was adjusted to $f_1=0.1, f_2=0.1, f_3=0.7, \theta =0.71$. The results for KL theory and homogeneously charged cylinder models coincide exactly.
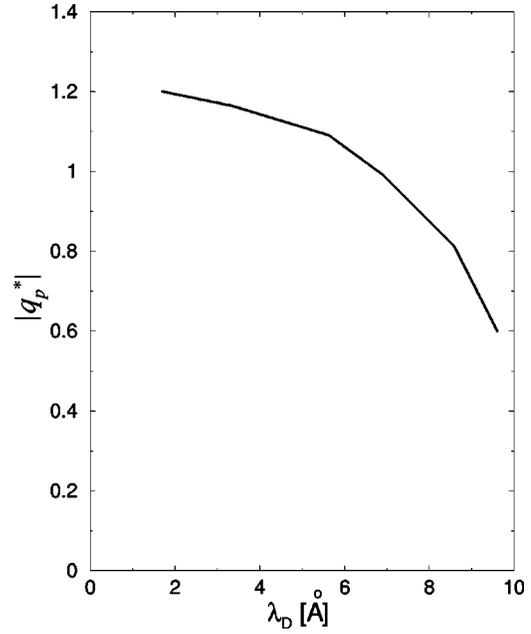
FIG. 17. Fitted renormalized phosphate charge q_p^* in the YS model versus the Debye screening length λ_D for runs D–H.

KL theory with a θ parameter corresponding to a width δ of one Bjerrum length and the homogeneously charged cylinder model give the same results. Again with a suitable scaling of the prefactor by introducing a renormalized phosphate charge q_p^*, respectively, by fitting the condensed fraction θ, one can achieve good agreement with the simulation data for distances larger than 24 Å. The fitting parameter q_p^* used for the YS model is $-1.1e$, while the optimal condensed fraction θ for the KL theory is 0.2. The optimal renormalized phosphate charge q_p^* is shown versus salt concentration in
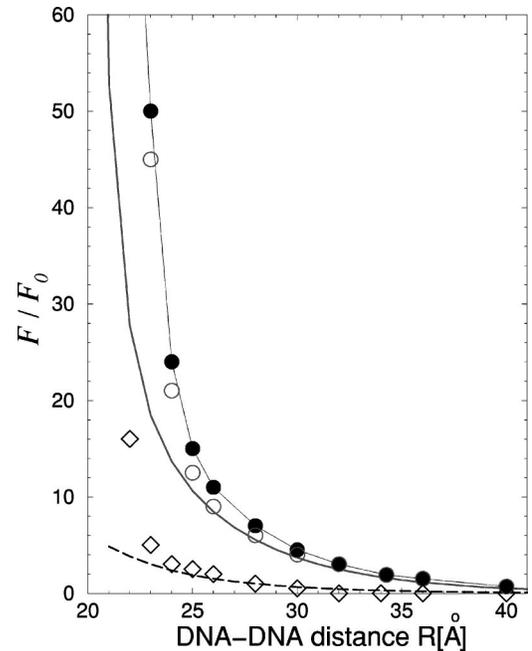
FIG. 18. Same as Fig. 9 but now for run I and $\phi=0°$, $\phi_0 =18°$. The KL theory was adjusted to $f_1=0.1, f_2=0.1, f_3=0.7, \theta =0.71$. Note that the KL and homogeneously charged cylinder models produce the same curves.

Fig. 17. Note that the usual DLVO size correction factor ζ is already incorporated in the interaction, so what one sees are actual deviations from the DLVO theory. The renormalized charge q_p^* increases with increasing C_s which is consistent with the works of Delrow *et al.* [73] and Stigter [27]. If one simulates the force within the homogeneously charged rod model, one finds good agreement with our simulation data for large separations. Consequently, the details of the charge pattern do not matter for large salt concentrations.

We also note that our simulations give no notable dependence of the force on the relative orientation ϕ for $h > 6$ Å. Only for small separations, $h < 6$ Å there is a slight dependence in agreement with Ref. [57].

Finally we show the influence of the ion and phosphate size on the effective force (for the parameters of run I) in Fig. 18. The electrostatic part of the force is now repulsive but the total force is still dominated by the depletion part. As far as the comparison to linear screening theories is concerned, one may draw similar conclusions as for Fig. 16. The fitting parameter q_p^* needed to describe the long-distance behavior within the YS model does not depend sensitively on the phosphate and ion sizes. With a suitable scaling of the prefactor one can achieve good agreement with the simulation data for distance larger than 26 Å. The fitting parameter q_p^* used for the YS model is $-1.1e$, while the optimal condensed fraction θ for the KL theory is 0.19. Here again, simulations of the homogeneously charged cylinder model are in good agreement with our results obtained for a double stranded DNA molecule.

IX. COMMENTS AND CONCLUSIONS

In conclusion, we have calculated the interaction between two parallel B-DNA molecules within a ''primitive'' model. In particular, we focused on the distance- and orientation-resolved effective forces and torques as a function of salt concentration. Our main conclusions are as follows.

First, the interaction force for larger separations is repulsive and dominated by microion depletion. The orientational dependence induced by the internal helical charge pattern is short-ranged decaying within a typical surface-to-surface separation of 6 Å. For shorter separations there is a significant dependence on the relative orientation ϕ and on the discreteness of the charge distribution along the strands. As a function of ϕ, the force can be both attractive and repulsive. This may lead to unusual phase behavior in smectic layers of parallel DNA molecules. Details of the molecular shape and counterion size are important for small separations as well. The torque is relatively small except for small separations where it exhibits a complicated ϕ dependence.

Second, as a function of added salt concentration we predict a nonmonotonic behavior of the force induced by a competition between delocalization of condensed counterions and enhanced electrostatic screening. This effect can in principle be verified in experiments.

Third, linear screening theories describe the simulation data qualitatively but not quantitatively. Having in mind that the total force is dominated by the depletion term which is typically neglected in linear screening theory, such theories need improvement. On the other hand, the different theories predict the correct long-distance behavior, if a phenomenological fit parameter—as the renormalized phosphate charge q_p^* for the Yukawa-segment model or the condensation fraction θ for the Kornyshev-Leikin model—is introduced. The Yukawa-segment model can even predict the orientational dependence of the force and the torque at smaller distances in the case of small counterion and phosphate sizes. Hence, a phenomenological Yukawa segment model can be used in a statistical description of the phase behavior of many parallel DNA strands in a smectic layer.

Future work should focus on an analysis for divalent counterions which are expected to lead to a qualitatively different behavior since the Coulomb coupling is enhanced strongly in this case. Also, one should step by step increase the complexity of the model in order to take effects such as dielectric discontinuities [38,41,27,99], chemical bindings of counterions in the grooves, and discrete polarizable solvents into account.

APPENDIX: LEKNER SUMMATION METHOD FOR FORCES

In our simulations we account for the long-range nature of the Coulomb interactions via the efficient method proposed by Lekner [68]. This method has been successfully applied to partially periodic systems [14,100]. For an assembly of N ions in a central cubic cell of dimension L, the Coulomb force $\vec{F}_i^{(c)}$ exerted onto particle i by particle j, and by all repetitions of particle j in the periodic system, is

$$\vec{F}_i^{(c)} = \frac{q_i q_j}{\epsilon} \sum_{\text{all cells}} \frac{\vec{r}_i - \vec{r}_j}{|\vec{r}_i - \vec{r}_j|^3}. \tag{A1}$$

Because of x, y, z symmetry it is sufficient to consider only one component of the force. For the x component of the force we have

$$\vec{F}_{ix}^{(c)} = \frac{q_i q_j}{\epsilon L^2} 8\pi \sum_{l=1}^{\infty} l \sin\left(2\pi l \frac{\Delta x}{L}\right) \sum_{m=-\infty}^{\infty} \sum_{n=-\infty}^{\infty}$$
$$\times K_0\left\{2\pi l\left[\left(\frac{\Delta y}{L} + m\right)^2 + \left(\frac{\Delta z}{L} + n\right)^2\right]^{1/2}\right\}. \tag{A2}$$

Here, $\Delta x = x_i - x_j$, $\Delta y = y_i - y_j$, $\Delta z = z_i - z_j$, and $K_0(z)$ is the modified Bessel function of zero order.

For a pair of particles not aligned parallel to the x axis, the convergence of the sum in Eq. (A2) is fast. Thus an evaluation of just 20 terms in the sum is enough to get a part-per-

million accuracy. The convergence becomes worse when simultaneously $|\Delta y| < \delta$ and $|\Delta z| < \delta (\delta \ll L)$ for the case $m = 0 = n$. The number of terms needed in the sum for a desired accuracy increases rapidly with increasing δ.

If the particles are aligned parallel to the x axis such that $|\Delta y| + |\Delta z| \equiv 0$, the sum in Eq. (A2) diverges with $m = 0 = n$. For this particular case $\vec{F}_{ix}$ is

$$\vec{F}_{ix}^{(c)} = \frac{q_i q_j}{\epsilon L^2} \frac{8\pi}{\sqrt{2}} \sum_{l=1}^{\infty} l \sin\left(2\pi l \frac{\Delta x}{2L}\right)$$
$$\times \sum_{m=-\infty}^{\infty} \left[K_0\left(2\pi l \left|\frac{\Delta x}{2L} + m\right|\right) + (-1)^l \right.$$
$$\left. \times K_0\left(2\pi l \left|\frac{\Delta x}{2L} + m - \text{sgn}(\Delta x)\frac{1}{2}\right|\right) \right]. \quad \text{(A3)}$$

[1] B. Jayaram and D.L. Beveridge, Annu. Rev. Biophys. Biomol. Struct. **25**, 367 (1996).

[2] B.H. Zimm and M. LeBret, J. Biomol. Struct. Dyn. **1**, 461 (1983).

[3] P.J. Lin-Chung and A.K. Rajagopal, Phys. Rev. E **52**, 901 (1995).

[4] M. LeBret and B.H. Zimm, Biopolymers **23**, 287 (1984).

[5] B.J. Klein and G.R. Pack, Biopolymers **22**, 2331 (1983).

[6] V.A. Bloomfield, Biopolymers **44**, 269 (1997).

[7] N. Grønbech-Jensen, R.J. Mashl, R.F. Bruinsma, and W.M. Gelbart, Phys. Rev. Lett. **78**, 2477 (1997); N. Grønbech-Jensen and K.M. Beardmore, Physica A **261**, 74 (1998).

[8] L.G. Nilsson, L. Gulbrand, and L. Nordenskiöld, Mol. Phys. **72**, 177 (1991).

[9] L. Guldbrand, B. Jönsson, H. Wennerström, and P. Linse, J. Chem. Phys. **80**, 2221 (1984).

[10] P.G. Bolhuis, T. Åkesson, and B. Jönsson, J. Chem. Phys. **98**, 8096 (1993).

[11] E. Allahyarov, I. D'Amico, and H. Löwen, Phys. Rev. Lett. **81**, 1334 (1998).

[12] N. Grønbech-Jensen, K.M. Beardmore, and P. Pincus, Physica A **261**, 74 (1998).

[13] A.P. Lyubartsev, J.X. Tang, P.A. Janmey, and L. Nordenskiöld, Phys. Rev. Lett. **81**, 5465 (1998).

[14] R.J. Mashl and N. Grønbech-Jensen, J. Chem. Phys. **109**, 4617 (1998); **110**, 2219 (1999).

[15] I. Rouzina and V.A. Bloomfield, J. Chem. Phys. **100**, 9977 (1996).

[16] R.W. Wilson and V.A. Bloomfield, Biochemistry **18**, 2192 (1979); R.W. Wilson, D.C. Rau, and V.A. Bloomfiled, Biophys. J. **30**, 317 (1980).

[17] J. Widom and R.L. Baldwin, J. Mol. Biol. **144**, 431 (1980).

[18] R. Kjellander, S. Marcelja, R.M. Pashley, and J.P. Quirk, J. Chem. Phys. **92**, 4399 (1990); H. Greberg and R. Kjellander, *ibid.* **108**, 2940 (1998).

[19] P. Kekicheff, S. Marcelja, T.J. Senden, and V.E. Shubin, J. Chem. Phys. **99**, 6098 (1993).

[20] G.M. Kepler and S. Fraden, Phys. Rev. Lett. **73**, 356 (1994).

[21] M.O. Khan and B. Jönsson, Biopolymers **49**, 121 (1999).

[22] N. Lee and D. Thirumalai, e-print cond-mat/9907199 (1999).

[23] M. Ueda and K. Yoshikawa, Phys. Rev. Lett. **77**, 2133 (1996).

[24] A.P. Lyubartsev and L. Nordenskiold, J. Phys. Chem. **99**, 10373 (1995).

[25] J. P. Hansen, H. Löwen, Annu. Rev. Phys. Chem. **51**, 209 (2000).

[26] B. Jayaram, K. Sharp, and B. Honig, Biopolymers **28**, 975 (1989).

[27] D. Stigter, Biopolymers **46**, 503 (1998).

[28] M. Troll, D. Roitman, J. Conrad, and B.H. Zimm, Macromolecules **19**, 1186 (1986).

[29] F.E. Karasz and T.L. Hill, Arch. Biochem. Biophys. **97**, 505 (1962).

[30] D.C. Rau, B. Lee, and V.A. Parsegian, Proc. Natl. Acad. Sci. U.S.A. **81**, 2621 (1984); R. Podgornik, D.C. Rau, and V.A. Parsegian, Biophys. J. **66**, 962 (1994); R. Podgornik, D.C. Rau, and V.A. Parsegian, Macromolecules **22**, 1780 (1989); H.H. Strey, V.A. Parsegian, and R. Podgornik, Phys. Rev. Lett. **78**, 895 (1997); D.C. Rau and V.A. Parsegian, Biophys. J. **61**, 246 (1992); R. Podgornik, H.H. Strey, K. Gawrisch, D.C. Rau, A. Rupprecht, and V.A. Parsegian, Proc. Natl. Acad. Sci. U.S.A. **93**, 4261 (1996); S. Leikin, V.A. Parsegian, D.C. Rau, and R.P. Rand, Annu. Rev. Phys. Chem. **44**, 369 (1993).

[31] S. Leikin, D.C. Rau, and V.A. Parsegian, Phys. Rev. A **44**, 5272 (1991).

[32] R.P. Rand, N. Fuller, V.A. Parsegian, and D.C. Rau, Biochemistry **27**, 7711 (1988).

[33] D.C. Rau and V.A. Parsegian, Biophys. J. **61**, 260 (1992).

[34] D.W.R. Gruen, S. Marcelja, and B.A. Pailthrope, Chem. Phys. Lett. **82**, 315 (1981).

[35] P. Mariani and L. Saturni, Biophys. J. **70**, 2867 (1996).

[36] J. Mazur and R.L. Jernigan, Biopolymers **31**, 1615 (1991).

[37] B.E. Hingerty, R.H. Ritchie, T.L. Ferrel, and J.E. Turner, Biopolymers **24**, 427 (1985).

[38] B. Jayaram, S. Swaminathan, D.L. Beveridge, K. Sharp, and B. Honig, Macromolecules **23**, 3156 (1990).

[39] G. Lamm and G.R. Pack, J. Phys. Chem. **101**, 959 (1997).

[40] A.V. Lukashin, D.B. Beglov, and M.D. Frank-Kamenetskii, J. Biomol. Struct. Dyn. **9**, 517 (1991).

[41] J.R.C. van der Maarel, Biophys. J. **76**, 2673 (1999).

[42] F. Fogolari, P. Zuccato, G. Esposito, and P. Viglino, Biophys. J. **76**, 1 (1999).

[43] K. Wagner, E. Keyes, T.W. Kephart, and G. Edwards, Biophys. J. **73**, 21 (1997).

[44] G.R. Pack, G.A. Garrett, L. Wong, and G. Lamm, Biophys. J. **65**, 1363 (1993).

[45] P. Mills, C.F. Anderson, and M.T. Record, J. Phys. Chem. **89**, 3984 (1985).

[46] S. Gavryushov and P. Zielenkiewicz, Biophys. J. **75**, 2732 (1998).

[47] C.S. Murthy, R.J. Bacquet, and P.J. Rossky, J. Phys. Chem. **89**, 701 (1985).

[48] V. Vlachy and A.D.J. Haymet, J. Chem. Phys. **84**, 5874 (1986).

[49] M.D. Paulsen, C.F. Anderson, and M.T. Record, Biopolymers **27**, 1249 (1988).

[50] G.R. Pack, L. Wong, and G. Lamm, Biopolymers **49**, 575 (1999).

[51] J. Granot, Biopolymers **22**, 1831 (1983).

[52] B.I. Shklovskii, Phys. Rev. Lett. **82**, 3268 (1999); V.I. Perel and B.I. Shklovskii, Physica (Amsterdam) **274A**, 446 (1999); T.T. Nguyen, I. Rouzina, and B.I. Shklovskii, J. Chem. Phys. **112**, 2562 (2000); B.I. Shklovskii, Phys. Rev. E **60**, 5802 (1999).

[53] Y. Levin, J.J. Arenzon, and J.F. Stilck, Phys. Rev. Lett. **83**, 2680 (1999); J.J. Arenzon, J. Stilck, and Y. Levin, Eur. Phys. J. B **12**, 79 (1999).

[54] A.V. Lukashin, D.B. Beglov, and M.D. Frank-Kamenetskii, J. Biomol. Struct. Dyn. **8**, 1113 (1991).

[55] J. Conrad, M. Troll, and B.H. Zimm, Biopolymers **27**, 1711 (1988).

[56] B. Jayaram and D.L. Beveridge, J. Phys. Chem. **94**, 4666 (1990).

[57] D. Hochberg, T.W. Kephart, and G. Edwards, Phys. Rev. E **49**, 851 (1994).

[58] G. Edwards, D. Hochberg, and T.W. Kephart, Phys. Rev. E **50**, R698 (1994).

[59] D. Hochberg, G. Edwards, and T.W. Kephart, Phys. Rev. E **55**, 3765 (1997).

[60] A.A. Kornyshev and S. Leikin, J. Chem. Phys. **107**, 3656 (1997).

[61] M. LeBret and B.H. Zimm, Biopolymers **23**, 271 (1984).

[62] J.L. Hecht, B. Honig, Y.K. Shin, and W. L. Hubbell, J. Phys. Chem. **99**, 7782 (1995).

[63] H. Löwen, J.P. Hansen, and P.A. Madden, J. Chem. Phys. **98**, 3275 (1993).

[64] E. Allahyarov, H. Löwen, and S. Trigger, Phys. Rev. E **57**, 5818 (1998).

[65] E. Allahyarov, I. D'Amico, and H. Löwen, Phys. Rev. E **60**, 3199 (1999).

[66] H. Löwen, Prog. Colloid Polym. Sci. **110**, 12 (1998).

[67] M.P. Allen and D.J. Tildesley, *Computer Simulation of Liquids* (Oxford University Press, Oxford, 1991).

[68] J. Lekner, Physica A **176**, 485 (1991); J. Lekner, Mol. Simul. **20**, 357 (1998).

[69] M.K. Gilson, K.A. Sharp, and B. Honig, J. Comput. Chem. **9**, 327 (1987).

[70] C. Schildkraut and S. Lifson, Biopolymers **3**, 195 (1965).

[71] J.M. Bailey, Biopolymers **12**, 559 (1973).

[72] M.T. Record, Biopolymers **5**, 975 (1967).

[73] J.J. Delrow, J.A. Gebe, and J.M. Schurr, Inc. Biopolymers **42**, 455 (1997).

[74] D. Soumpasis, J. Chem. Phys. **69**, 3190 (1978).

[75] E.J.W. Vervey and J.T.G. Overbeek, *Theory of Stability of Lyophobic Colloids* (Elsevier, Amsterdam, 1948).

[76] H. Löwen, J. Chem. Phys. **100**, 6738 (1994).

[77] H. Löwen, P.A. Madden, and J.-P. Hansen, Phys. Rev. Lett. **68**, 1081 (1992).

[78] A.A. Kornyshev and S. Leikin, Proc. Natl. Acad. Sci. U.S.A. **95**, 13579 (1998).

[79] A.A. Kornyshev and S. Leikin, Biophys. J. **75**, 2513 (1998).

[80] A.A. Kornyshev and S. Leikin, Phys. Rev. Lett. **82**, 4138 (1999).

[81] A.A. Kornyshev and S. Leikin, Phys. Rev. E **62**, 2576 (2000).

[82] G.S. Manning, Q. Rev. Biophys. **11**, 179 (1978).

[83] J. Ray and G.S. Manning, Biopolymers **32**, 541 (1992).

[84] M.L. Bleam, C.F. Anderson, and M.T. Record, Biochemistry **22**, 5418 (1983).

[85] S. Padmanabhan, B. Richey, C.F. Anderson, and M.T. Record, Biochemistry **27**, 4367 (1988).

[86] M.K. Gilson, M.E. Davis, B.A. Luty, and J.A. McCammon, J. Phys. Chem. **97**, 3591 (1993).

[87] J.C.G. Montoro and J.L.F. Abascal, J. Chem. Phys. **103**, 8273 (1995).

[88] X. Shui, L. McFail-lsom, G.G. Hu, and L.D. Williams, Biochemistry **37**, 8341 (1998).

[89] X. Shui, G. Sines, L. McFail-lsom, D. Van-Derveer, and L.D. Williams, Biochemistry **37**, 16 877 (1998).

[90] L. McFail-lsom, C.C. Sines, and L.D. Williams, Curr. Opin. Struct. Biol. **9**, 298 (1999).

[91] N.V. Hud, V. Sklenar, and J. Feigon, J. Mol. Biol. **285**, 233 (1999).

[92] N.V. Hud, P. Schultze, and J. Feigon, J. Am. Chem. Soc. **120**, 6403 (1998).

[93] M.A. Young, B. Jayaram, and D.L. Beveridge, J. Am. Chem. Soc. **119**, 59 (1997).

[94] M.A. Young and D.L. Beveridge, J. Mol. Biol. **281**, 675 (1998).

[95] S. Alexander, P.M. Chaikin, P. Grant, G.J. Morales, P. Pincus, and D. Hone, J. Chem. Phys. **80**, 5776 (1984).

[96] G.S. Manning, Acc. Chem. Res. **12**, 443 (1979).

[97] M.T. Record, C.F. Anderson, and T.M. Lohman, Q. Rev. Biophys. **11**, 103 (1978).

[98] M. Gueron and G. Weisbuch, Biopolymers **19**, 353 (1980).

[99] J. Skolnick and M. Fixman, Macromolecules **10**, 944 (1977); **11**, 867 (1978).

[100] N. Grønbech-Jensen, G. Hummer, and K.M. Beardmore, Mol. Phys. **92**, 941 (1997).